

Title	Growth process, characterization, and modeling of electronic properties of coupled InAsSbP nanostructures
Author(s)	Marquardt, Oliver; Hickel, Tilmann; Neugebauer, Joerg; Gambaryan, Karen M.; Aroutiounian, Vladimir M.
Publication date	2011
Original citation	Marquardt, O., Hickel, T., Neugebauer, J., Gambaryan, K. M. and Aroutiounian, V. M. (2011) 'Growth process, characterization, and modeling of electronic properties of coupled InAsSbP nanostructures', Journal of Applied Physics, 110(4), 043708 (6pp). doi: 10.1063/1.3624621
Type of publication	Article (peer-reviewed)
Link to publisher's version	http://aip.scitation.org/doi/10.1063/1.3624621 http://dx.doi.org/10.1063/1.3624621 Access to the full text of the published version may require a subscription.
Rights	© 2011, American Institute of Physics. This article may be downloaded for personal use only. Any other use requires prior permission of the author and AIP Publishing. The following article appeared in Marquardt, O., Hickel, T., Neugebauer, J., Gambaryan, K. M. and Aroutiounian, V. M. (2011) 'Growth process, characterization, and modeling of electronic properties of coupled InAsSbP nanostructures', Journal of Applied Physics, 110(4), 043708 (6pp). doi: 10.1063/1.3624621 and may be found at http://aip.scitation.org/doi/10.1063/1.3624621
Item downloaded from	http://hdl.handle.net/10468/4734

Downloaded on 2018-08-23T20:27:17Z

Growth process, characterization, and modeling of electronic properties of coupled InAsSbP nanostructures

Oliver Marquardt^{*}, Tilmann Hickel, Jörg Neugebauer, Karen M. Gambaryan, and Vladimir M. Aroutiounian

Citation: *Journal of Applied Physics* **110**, 043708 (2011); doi: 10.1063/1.3624621

View online: <http://dx.doi.org/10.1063/1.3624621>

View Table of Contents: <http://aip.scitation.org/toc/jap/110/4>

Published by the *American Institute of Physics*

AIP | Journal of
Applied Physics

Save your money for your research.
It's now **FREE** to publish with us -
no page, color or publication charges apply.

Publish your research in the
Journal of Applied Physics
to claim your place in applied
physics history.

Growth process, characterization, and modeling of electronic properties of coupled InAsSbP nanostructures

Oliver Marquardt,^{1,a)} Tilmann Hickel,¹ Jörg Neugebauer,¹ Karen M. Gambaryan,² and Vladimir M. Aroutiounian²

¹Max-Planck Institut für Eisenforschung, Max-Planck-Straße 1, D-40237 Düsseldorf, Germany

²Department of Physics of Semiconductors and Microelectronics, Yerevan State University, 1 A. Manoukian Str., Yerevan 0025, Armenia

(Received 19 April 2011; accepted 1 July 2011; published online 22 August 2011)

Quaternary III-V InAsSbP quantum dots (QDs) have been grown in the form of cooperative InAsSb/InAsP structures using a modified version of the liquid phase epitaxy. High resolution scanning electron microscopy, atomic force microscopy, and Fourier-transform infrared spectrometry were used to investigate these so-called nano-camomiles, mainly consisting of a central InAsSb QD surrounded by six InAsP-QDs, that shall be referred to as leaves in the following. The observed QDs average density ranges from 0.8 to $2 \times 10^9 \text{ cm}^{-2}$, with heights and widths dimensions from 2 to 20 nm and 5 to 45 nm, respectively. The average density of the leaves is equal to $(6-10) \times 10^9 \text{ cm}^{-2}$ with dimensions of approx. 5 to 40 nm in width and depth. To achieve a first basic understanding of the electronic properties, we have modeled these novel nanostructures using second-order continuum elasticity theory and an eight-band $\mathbf{k} \cdot \mathbf{p}$ model to calculate the electronic structure. Our calculations found a clear localization of hole states in the central InAsSb dot. The localization of electron states, however, was found to be weak and might thus be easily influenced by external electric fields or strain. © 2011 American Institute of Physics. [doi:10.1063/1.3624621]

I. INTRODUCTION

Narrow bandgap III-V semiconductor materials like InAs, GaSb, InSb, and their ternary and quaternary alloys are of particular interest to access mid- and far-infrared wavelength regions. These materials are promising for a new generation of LEDs, lasers and photodiodes for applications such as infrared gas sensors, for molecular spectroscopy, thermal imaging, photovoltaic and thermo-photovoltaic cells, as well as for several other infrared applications.

The absorption of infrared radiation in such devices based on direct bandgap semiconductor materials depends on the material used. The resulting number of photons per second per Watt is directly proportional to the wavelength. Since these materials utilize direct transitions of electrons, they have a high response speed compared with thermal detectors.¹ Correspondingly, they are highly interesting for various applications where such a high response speed detector system is needed. More efficient alternatives to direct band-gap detectors are based on the intersubband transitions in quantum-confined heterostructures. The advantage of such a quantum well infrared photodetector (QWIP) approach is the availability of a mature III-V fabrication technology and multi-spectral capability. Such heterostructures have a narrow absorption spectrum that can be tuned by varying the quantum well width and the barrier layer composition.

The most recent development in the field of infrared photodetectors is the normal incidence quantum-dot photodetector (QDIP) technique² in semiconductors such as

InGaAs/InP, InGaAs/GaAs, InSb/InAs, or SiGe/Si. These and other QD-based devices are expected to perform well at elevated temperatures due to their three-dimensional carrier confinement characteristics.³⁻⁵ In these low dimensional structures, the movement of charge carriers is constrained by potential barriers. QDIPs are inherently sensitive to normal incidence radiation and also the dark current is much lower than that of QWIPs. This technology will be useful in remote sensing, chemical and biological detection applications, as well as in photovoltaic (PV)⁶ and thermo-PV (TPV) cells.⁷

Among the III-V quaternary material systems, InAsSbP is a promising candidate because it can cover the very important mid-infrared region from 3 to 5 μm , adjusting its alloy composition with the three group-V elements only. This fact together with a potentially lattice-matched growth on an InAs substrate makes InAsSbP unique in this material class. While InAsSbP quantum dots have been successfully grown previously,^{3,7,8} only a few studies on quaternary cooperative QDs/leaves structures, so-called nano-camomiles, have been reported so far.^{4,5} In particular, while charge carrier localization is expected in the central InAsSb-QD rather than in the surrounding InAsP-leaves in these nano-camomiles, due to the conduction and valence band offsets of the dot, leaves and surrounding matrix material, long-ranged strain, and polarization potentials arising from the leaves are expected to induce a significant influence on the properties of the electrons and holes in the central dot. Controlling the composition ratio between As, Sb, and P allows strain control in InAsSbP, and therefore a modification of the growth process and structural properties of the InAsSb dots and the surrounding InAsP-leaves.

The previously observed nano-camomiles^{4,5} are furthermore an excellent subject for understanding the complicated

^{a)}Electronic mail: oliver.marquardt@tyndall.ie. Now at: Tyndall National Institute, Lee Maltings, Cork, Ireland.

influences of strain, polarization potential, and band offsets on the electronic structure of coupled InAsSb/InAsP nanostructures. To achieve a more detailed understanding of the electronic properties of these nanostructures, a theoretical description based on the experimental observations is required, allowing to study the influence of experimentally tunable parameters of the InAsSb/InAsP-nanostructures on their electronic properties and to identify possible applications of these systems.

In this paper, we present a combined experimental and theoretical study of coupled InAsSb/InAsP nanostructures, including their nucleation process and the optoelectronic properties. As a first approach to the electronic properties, we have chosen an eight-band $\mathbf{k} \cdot \mathbf{p}$ model including strain and built-in electrostatic potentials to calculate single-particle electron and hole states and their eigenenergies.

II. EXPERIMENTAL SETUP

The main driving force of InAsSb/InAsP-QD molecules is the surface diffusion of antimony atoms, similar to that in classic InAs/InSb-systems.⁹ This leads to the formation of InAsSb-QDs. Simultaneously, phosphorous atoms move in the surrounding material around the InAsSb-QD, thus forming the surrounding InAsP-QDs, that we refer to as leaves, and therefore forming a coupled InAsSb/InAsP dot-leaf-nanostructure without a wetting layer. The surface diffusion of phosphorous atoms to one or opposite directions opens up a new possibility and can be employed as an additional tool to control the nucleation process and the type of nanostructure which is grown. The resulting nanostructure can afterwards be buried in InAs, if required for the purpose of a specific device. Depending on the growth conditions, i.e., growth temperature, composition of the liquid phase and its contact time with the substrate surface, the geometry of the nanostructure changes. When the phosphorous atoms are energetically preferred to jump and are forced out of the QD, the InAsP-leaves will nucleate around the QD.^{4,5} Otherwise, when the phosphorous atoms are energetically preferred to move to the center of the QD, the final shape of the nanostructure will have the form of a quantum ring, i.e., a ring-like InAsSb-QD with a InAsP-QD on the top. In this case quantum rings are not surrounded by additional leaves. The size of the observed QD-nanostructures is influenced by the contact time of the liquid with the InAs surface, as the late stages of the growth process are typically characterized by an increase of larger QDs as they absorb smaller QDs. This behavior is commonly known as Ostwald ripening¹⁰ and leads to the formation of larger, ellipsoidal InAsSb-clusters that are observed and discussed in Ref. 4. A step-cooling version of liquid phase epitaxy (LPE) with a modified slide-boat crucible is applied for the nucleation of InAsSb/InAsP cooperative nanostructures. In that crucible, nucleation of the quantum-size objects and epitaxial films is performed from the thin (tunable from 200 to 500 μm in height) liquid phase in order to prevent the influence of convection and temperature gradient on the growth process. Our investigations show that this technological approach increases the reproducibility of the grown structures. According to the InAs-InSb-InP

quasi-ternary phase diagram,¹¹ as a starting point we use the quaternary liquid phase composition that corresponds to the InAs_{0.742} Sb_{0.08} P_{0.178} alloy in solid phase, that is conveniently lattice-matched to InAs substrate. We use the liquid phase supersaturated by both antimony and phosphorus to achieve a nucleation of InAsSb/InAsP dot/leaf-nanostructures. Other technological conditions are described in more detail in Refs. 4 and 8. In contrast to other growth techniques as molecular beam epitaxy or metal organic chemical vapor deposition, LPE operates comparatively closer to the thermodynamic equilibrium. To ensure a high purity of the epitaxial layers, the entire growth process has been performed under a pure hydrogen atmosphere. The InAs substrates used in this work were 11 mm in diameter, (100)-oriented, undoped, and have a background electron concentration of $2 \times 10^{16} \text{ cm}^{-3}$. High resolution SEM (SEM-EDXA-FEI Nova 600-Dual Beam) and AFM (TM Microscopes Autoprobe CP) techniques are used for the investigation and characterization of the QDs and leaves morphology, dimensions and distribution density. The Fourier-transform infrared spectrometry (FTIR-Nicolet/NEXUS) is used to investigate the transmission spectra of QD-leaf cooperative structures.

III. CALCULATION OF ELECTRONIC PROPERTIES

The energies of the conduction and valence band edges of InAs, InSb, InP, and their ternary alloys indicate highly interesting electronic properties of InAsSb/InAsP-alloy nanostructures. In particular, the band offsets of InSb in InAs suggest that electrons might be located in InAs, whereas the valence band maximum is inside InSb and thus makes this material to be preferred by the hole states. Based on these insights and further experimental information available, we have performed continuum model calculations to predict the elastic and electronic properties of coupled dot/leaf nanostructures and to identify possible ways to control their electro-optical behavior. Our studies are aiming at a general understanding of the unique properties of these systems, allowing a qualitative, rather than a fully quantitative comparison with the experimentally observed data. We have calculated the elastic properties of the system using second-order continuum elasticity theory,¹² similarly to our previous work on, e.g., nonpolar GaN/AlN quantum dots.¹³ From the obtained strain fields, the built-in polarization potential has been calculated. For this purpose, we have employed a plane-wave based formulation of the continuum elasticity theory, for details see Ref. 14. Lattice, elastic, and piezoelectric constants taken from Ref. 15 have been linearly interpolated between the InAs/InSb and InAs/InP parameters within the segregation profiles assumed in the present study.

Strain and built-in piezoelectric potentials enter the eight-band $\mathbf{k} \cdot \mathbf{p}$ Hamiltonian and thus modify the electronic structure of the nanostructure.¹⁶ The details of our plane-wave based implementation of the eight-band $\mathbf{k} \cdot \mathbf{p}$ formalism can again be found in Ref. 14. Moreover, we have previously evaluated the validity of the employed model for GaN/AlN QDs of smaller characteristic dimensions and were able to achieve an excellent agreement with atomistic tight-binding calculations.¹⁷ The parameters required for the calculation of

the electronic properties were also taken from Ref. 15. All parameters except for the bandgap were linearly interpolated between the corresponding binary alloys. For the bandgap, a strong bowing is observed in $\text{InAs}_{1-x}\text{Sb}_x$. This bandgap bowing reduces the conduction band offset of InAsSb for an Sb content of 20% such that it is smaller than the bulk InAs bandgap and thus potentially allows for a localization of electrons inside the InAsSb dot. The bandgap E_g is thus calculated in a quadratic interpolation

$$E_g(\text{InAs}_{1-x}\text{Sb}_x) = x \cdot E_g(\text{InSb}) + (1-x) \cdot E_g(\text{InAs}) - x \cdot (1-x) \cdot b_p(\text{InAsSb}), \quad (1)$$

where b_p is the bandgap bowing parameter that can also be found in Ref. 15.

IV. RESULTS

The high resolution SEM images of the InAsSbP QD/leaf cooperative structures and an enlarged view of these nano-camomiles are presented in Fig. 1. The observed QDs average density ranges from 0.8 to $2 \times 10^9 \text{ cm}^{-2}$, with heights and widths dimensions from 2 to 20 nm and 5 to 45 nm , respectively. The average density of the leaves is equal to 6 to $10 \times 10^9 \text{ cm}^{-2}$ with dimensions of approx. 5 to 40 nm in width and depth. Note that a bimodal growth mechanism for both the QDs and the leaves nucleation was observed. A Lifshits-Slezov-like distribution for the number of relatively small and lens-shaped QDs and leaves versus their average diameter was observed. Together with the nano-camomiles shown in Fig. 1, larger, ellipsoidal InAsSb -QDs have been observed, that do not exhibit surrounding InAsP -leaves, arising in the late stages of the growth process due to Ostwald ripening. However, these structures are not subject of the present work. More detailed descriptions, technological conditions and the nucleation mechanism of the InAsSbP quaternary QDs and the QD/leaf cooperative structures are presented in Refs. 4, 5, and 8.

The room temperature FTIR spectrum of uncapped InAsSbP QD/leaf structures grown on $\text{InAs}(100)$ by LPE is

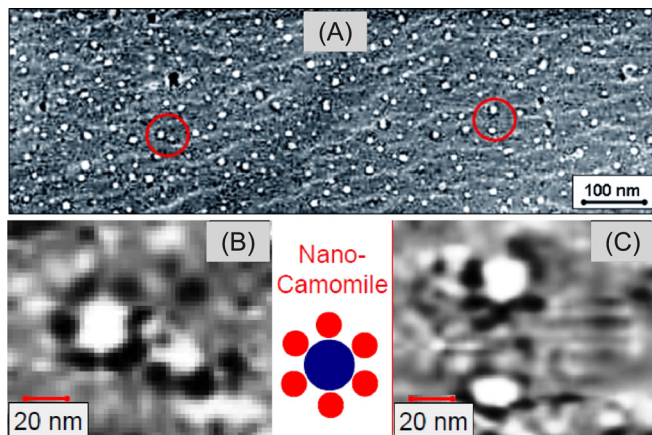


FIG. 1. (Color online) High resolution SEM images of the InAsSbP QD/leaf cooperative structures (A). (B) and (C): enlarged view of the nano-camomiles. White ovals are QDs, black ovals are leaves.⁴ A schematic picture is shown in the center.

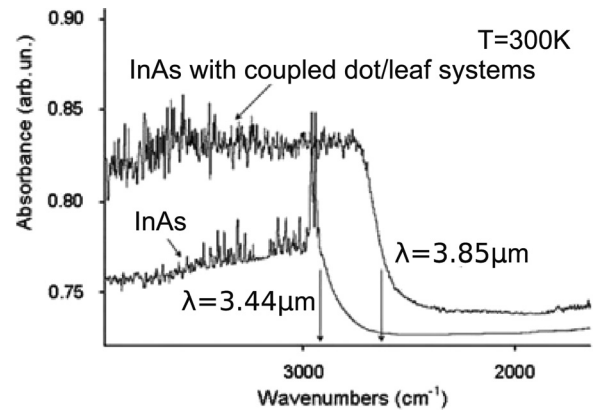


FIG. 2. FTIR spectra of the InAs test sample and the InAsSbP QD/leaf structure sample.⁴

presented in Fig. 2. As a test sample, we use the same undoped $\text{InAs}(100)$ substrate without InAsSb QDs and surrounding InAsP -leaves. The results show the displacement of the absorption edge toward the long wavelength region from $\lambda = 3.44 \mu\text{m}$ (for test sample) to $\lambda = 3.85 \mu\text{m}$. We assume that this effect is the result of the absorption by the QDs through the permitted energy sub-band. Even though the shift of the absorption edge clearly indicates the optical activity of the nanostructures, discrete emission peaks, are not clearly distinguishable in the spectrum. We account this to the fact that the spectrum was measured at room temperature and to the presence of the larger, ellipsoidal QDs that were reported in Ref. 8. Future investigations of the $\text{InAsSb}/\text{InAsP}$ -nanostructures will therefore require low-temperature photoluminescence measurements.

A. Modeling the electronic properties of InAsSbP -dot/leaf-molecules

To gain a more detailed insight in the elastic and electronic structure of the observed dot/leaf-nanostructures, we have carried out continuum elasticity and $\mathbf{k} \cdot \mathbf{p}$ -calculations. As our previously evaluated SEM-EDXA measurements have shown,^{4,8} the QDs are enriched by antimony atoms, whereas the leaves are enriched by phosphorus atoms. As a model system, we have therefore chosen an InAsSb QD surrounded by six InAsP leaves. The InAsSb dot has a flat, lens-like shape with a diameter of 18 nm and a height of 7.2 nm , which corresponds to the smaller dots observed in the above references. Furthermore, following experimental evidence from strain measurements at the QD interfaces,⁸ we have assumed the Sb content in the dots to have a maximum in the outer shell and to linearly decrease to the center with the Sb concentration being zero in the center of the dot and 20% in the shell region. This assumption of the composition profile serves as a first approach to understand the elastic and electronic properties of these systems. To gain more information about the composition profile in these $\text{InAsSb}/\text{InAsP}$ -nanostructures, further experiments such as high resolution transmission electron microscopy (HRTEM) are required, that have not been performed so far. For the six surrounding InAsP leaves, the composition profile behaves similarly. We again assume a maximum P content of 15% in the shell

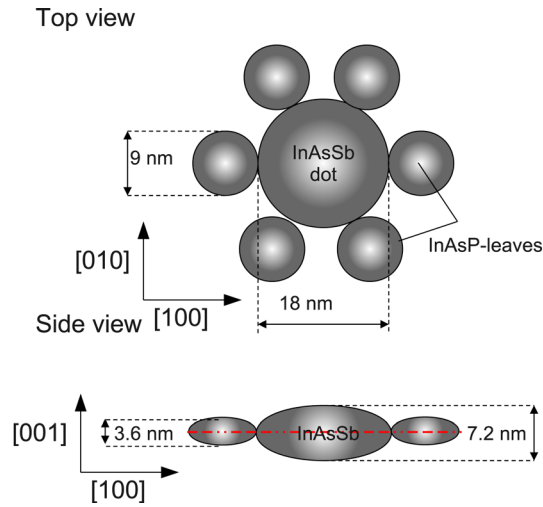


FIG. 3. (Color online) Top and side view of the lens-shaped InAsSb/InAsP QD molecule. For the half-lens-shaped molecule, the structure is cut in half in the middle perpendicular to the growth direction, marked by a dash-dotted red line in the side view.

region and pure InAs in the center. The diameter of the leaves is chosen to be 9 nm and the height is 3.6 nm, according to the experimental observations of the smaller dot/leaf systems.

The experimental information from Fig. 1 and Refs. 4 and 5 allow moreover lens-shaped coupled InAsSb/InAsP QD molecules, i.e., the full lens-shaped dots and leaves might likewise be cut in half perpendicular to the growth direction. We have therefore simulated both possible structures, i.e., half-lens-shaped as well as full-lens-shaped dot/leaf systems in our calculations, in both cases a wetting layer was not considered, following experimental observations. The QD molecule geometry is depicted in Fig. 3. We have, furthermore, considered buried QD/leaf-systems in this study.

The bulk conduction and valence band edges of a lens-shaped dot/leaf system, resulting from the assumed material composition and the bulk band offsets, are shown in Fig. 4 along the [010]-direction through the dot's center. With a shallow conduction band minimum being located in the outer

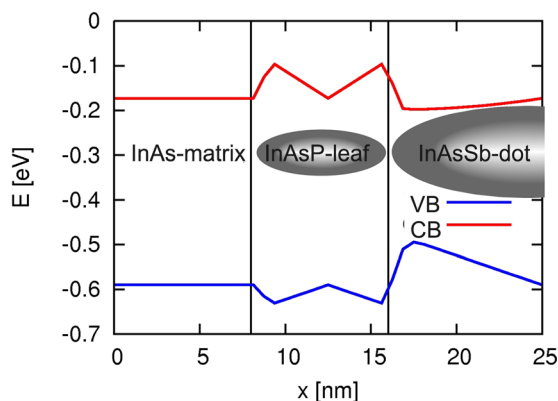


FIG. 4. (Color online) Bulk conduction (red, light gray) and valence band (blue, dark gray) offset along the [010]-direction from the boundary to the center of the system. The InAsP leaves and InAsSb dots are indicated as ellipsoids where dark (light) gray indicates high (low) P or Sb content (color online).

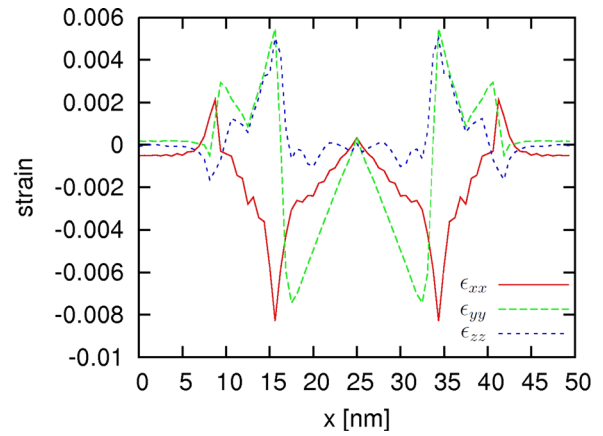


FIG. 5. (Color online) Diagonal components of the strain tensor plotted along the [010]-direction through the center of the dot and two leaves.

regions of the central InAsSb-dot, localized electron states can possibly be expected in the dots. However, the bulk band edges are qualitatively modified if strain is taken into account. The diagonal strain components in the full-lens-shaped QD molecule systems are plotted along the [010]-direction in Fig. 5. As can be seen in Fig. 6, strain, derived from a second-order continuum elasticity model, has a significant influence on the conduction and valence band offsets. In particular, the shallow minimum of the conduction band in the InAsSb dot shell vanishes, as due to strain the conduction band offset in the outer InAsSb-shell is increased to a value higher than the one in bulk InAs, such that a localization of electrons inside the dot cannot be expected any more. The valence bands are additionally split up due to strain. However, since the valence band maximum remains inside the InAsSb shell, the hole state localization is not expected to be qualitatively modified and holes are expected to localize similarly to the case where strain is neglected.

All of the above investigations were performed for the full-lens-shaped dot/leaf molecule. The half-lens-shaped structure behaves qualitatively similar. The built-in piezoelectric

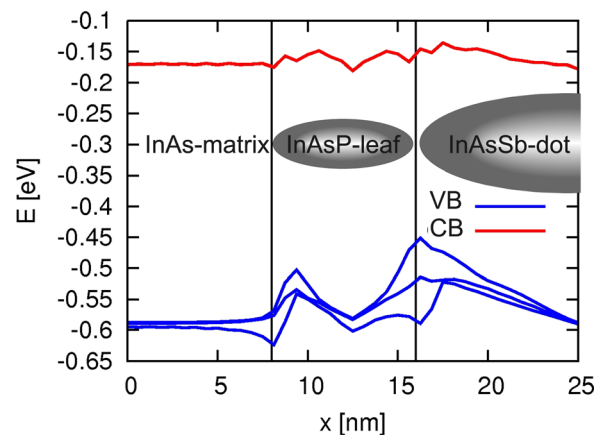


FIG. 6. (Color online) Conduction (red, light gray) and valence band (blue, dark gray) offsets modified by strain and built-in electrostatic potentials plotted along the [010]-direction from the boundary to the center of the system (color online). The three highest valence bands are split due to strain. Minor numerical wiggles occur around the dot and leaves boundaries due to abrupt interfaces occurring in these regions.

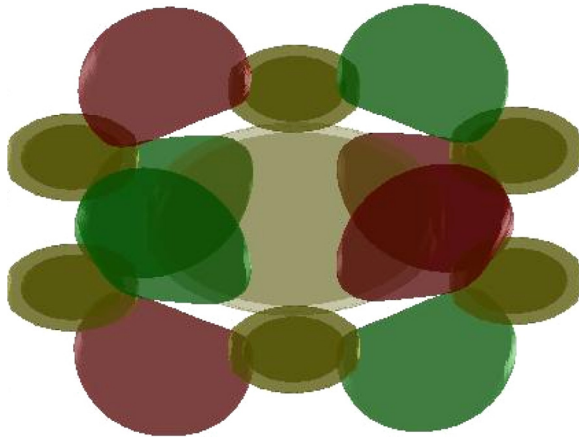


FIG. 7. (Color online) Polarization potential of the InAsSb-dot/InAsP leaves molecule in a 3D view. Bright (dark) yellow isosurfaces with sixfold symmetry mark the central dot (surrounding leaves). The red and green isosurfaces exhibiting a twofold symmetry mark a potential of 60:17 mV.

potential of the dot/leaf-molecule has been calculated from the strains as described in Ref. 14 and is shown in Fig. 7. Maximum and minimum of the potential are at around ± 33 mV, however, these extrema were found to occur outside the central dot and are thus not expected to induce significant modifications of the electron and hole state localization. Moreover, it is clearly visible that the hexagonal symmetry of the InAsSb dot with the surrounding InAsP leaves is not reflected in the resulting polarization potential that shows the qualitative behavior of comparable (001)-grown, flat lens-shaped dots in a zinc blende structure. We conclude, that the symmetry of the polarization potential is thus dominated by the underlying crystal structure rather than by the nanostructure's shape.

The shallow minima of the conduction band, that vanish if strain is considered in the model system as well as the modifications that occur for the valence band suggest a weak localization of the electrons whereas a localization of holes inside the InAsSb dot can be expected. The electron and hole states closest to the bandgap were thus calculated using an eight-band $\mathbf{k} \cdot \mathbf{p}$ model. To understand the influence of strain on the electron localization, we have again first performed these calculations neglecting strain and built-in potentials. Under these assumptions, we have found the electron ground state to localize inside the InAsSb dot, as can be seen in Fig. 8 for the full-lens-shaped nano-camomile. Moreover, we found the hole states to be strongly localized in the outer InAsSb dot shell.

If we take the previously computed strains and polarization potentials into account, we find the hole states still localized in the dot's shell region. However, the electrons in this case were found to be no longer localized in the dot. It is therefore clear that the shallow conduction band minimum in InAsSb is modified by strain resulting from both the QD material and the surrounding leaves such that it does not allow for electrons to localize inside the dot. The above results apply to the full-lens-shaped dot, however, no qualitative change is observed for the half-lens-shaped system and the eigenenergies show a similar quantitative behavior. The electron and hole eigenenergies for the full and the half-lens-shaped system are shown in Table I. As these single-particle

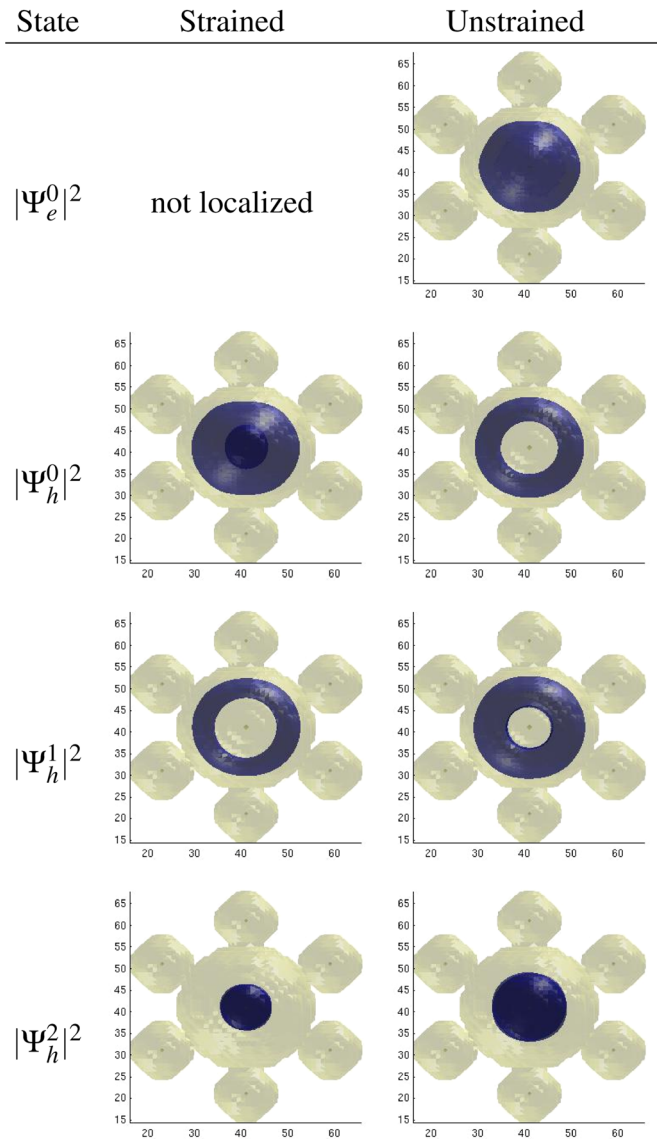


FIG. 8. (Color online) Electron ground state and hole states closest to the bandgap for model calculations including (left) and excluding (right) the modification of the bulk electronic properties due to strain. The QD-molecule is marked yellow (light gray). Blue (dark gray) isosurfaces represent 50% of the maximum charge density for the hole states and 90% for the electron state.

calculations do not include excitonic effects and are furthermore performed under the assumption of a temperature of 0K, we cannot expect an exact agreement with the FTIR-spectrum shown in Fig. 2. The electron-hole ground state energy difference corresponds to wave lengths of $3.72 \mu\text{m}$ for the half-lens-shaped QD and $3.64 \mu\text{m}$ for the full-lens-shaped dot, however, which is close to the measured absorption band edge in Fig. 2. The absolute energies of electrons and holes are modified due to strain by a few meV only. However, it can be seen that strain and polarization potentials break degeneracies that occur when such effects are not included. In particular the polarization potential will induce an energy splitting of states that may be degenerate due to the lack of the bulk-inversion asymmetry in the employed eight-band $\mathbf{k} \cdot \mathbf{p}$ -model.¹⁸ On the other hand, the fundamental question if a hole state close to the valence band

TABLE I. Electron and hole eigenenergies in eV. $\Psi_{e/h}$ denote electron/hole wave functions.

State	Full-lens-shaped	
	Strained	Unstrained
Ψ_e^0	-0.1704	-0.1741
Ψ_h^0	-0.5125	-0.5024
Ψ_h^1	-0.5136	-0.5048
Ψ_h^2	-0.5140	-0.5053
Ψ_h^3	-0.5140	-0.5077
	Half-lens-shaped	
Ψ_e^0	-0.1716	-0.1729
Ψ_h^0	-0.5048	-0.4927
Ψ_h^1	-0.5067	-0.4941
Ψ_h^2	-0.5067	-0.4970
Ψ_h^3	-0.5082	-0.4975

maximum is localized in the InAsSb dot or outside is not affected by this simplification.

V. SUMMARY

We have performed a first joint experimental and theoretical investigation of quaternary QD molecules consisting of InAsSbP in the form of cooperative InAsSb-dot-InAsP QD structures grown by a modified version of the LPE. Our theoretical studies of the electronic structure of these InAsSb/InAsP nanostructures have revealed a strong localization of hole states in the InAsSb dot. The electron localization, however, was found to be easily influenced by minor effects as, e.g., strain. This behavior results from the conduction band offset of InAsSb which decreases below the InAs bulk conduction band offset only slightly due to a strong bandgap bowing. This results in a shallow barrier for the electrons which can be easily overcome by strain or additional electric fields. This property makes these ternary QD molecules highly attractive for applications where an access to the electron localization via external electric fields or applied strain is required. It is therefore necessary to achieve a more detailed understanding of the structures studied

within this work from both experimental and theoretical side and to gain a better insight into their properties, such as, e.g., accurate segregation profiles obtained from HRTEM measurements and the electronic and optical properties that can be predicted from many-particle calculations and measured from photoluminescence spectra.

ACKNOWLEDGMENTS

The authors wish to thank Prof. Dr. R. Fornari, Dr. T. Boeck from Leibniz Institute for Crystal Growth (IKZ, Berlin), and Ms. M. Schulze (now at Bosch AG) for SEM and AFM measurements. Parts of this work have been carried out in the frames of the Armenian National Governmental Program for Nano-Electronics and of the ISTC grant A-1232.

- ¹A. Rogalski, *Acta Physica Polonica A* **116**, 389 (2009).
- ²P. Bhattacharya, X. H. Su, S. Chakrabarti, G. Ariyawansa, and A. G. U. Perera, *J. Appl. Phys.* **86**, 191106 (2005).
- ³A. Krier, Z. Labadi, and A. Hammiche, *J. Phys. D: Applied Physics* **32**, 2587 (1999).
- ⁴K. M. Gambaryan, *Nanoscale Research Letters* **5**, 587 (2010).
- ⁵V. M. Aroutiounian, K. M. Gambaryan, and P. G. Soukiassian, *Surf. Sci.* **604**, 1127 (2010).
- ⁶V. M. Aroutiounian, S. G. Petrosian, A. Khachatryan, and K. Touryan, *J. Appl. Phys.* **89**, 2268 (2001).
- ⁷K. M. Gambaryan, V. M. Aroutiounian, T. Boeck, and M. Schulze, *Phys. Status Solidi (c)* **6**, 1456 (2009).
- ⁸K. M. Gambaryan, V. M. Aroutiounian, T. Boeck, M. Schulze, and P. G. Soukiassian, *J. Phys. D: Applied Physics (FTC)* **41**, 162004 (2008).
- ⁹K. D. Moiseev, Y. A. Parkhomenko, A. V. Ankudinov, E. V. Gushchina, M. P. Mikhailova, A. N. Titkov, and Y. P. Yakolev, *Tech. Phys. Lett.* **33**, 295 (2007).
- ¹⁰R. D. Vengrenovich, Y. V. Gudyma, and S. V. Yarema, *Semiconductors* **35**, 1378 (2001).
- ¹¹K. Onabe, *NEC Res. Develop.* **72**, 1 (1984).
- ¹²M. Povolotskyi, M. auf der Maur, and A. D. Carlo, *Phys. Status Solidi (c)* **2**, 3891 (2005).
- ¹³O. Marquardt, T. Hickel, and J. Neugebauer, *J. Appl. Phys.* **106**, 083707 (2009).
- ¹⁴O. Marquardt, S. Boeck, C. Freysoldt, T. Hickel, and J. Neugebauer, *Computer Phys. Commun.* **181**, 765 (2010).
- ¹⁵I. Vurgaftman, J. R. Meyer, and L. R. R. Mohan, *J. Appl. Phys.* **89**, 5815 (2001).
- ¹⁶T. B. Bahder, *Phys. Rev. B* **41**, 11992 (1990).
- ¹⁷O. Marquardt, D. Mourad, S. Schulz, T. Hickel, G. Czycholl, and J. Neugebauer, *Phys. Rev. B* **78**, 235302 (2008).
- ¹⁸G. Bester and A. Zunger, *Phys. Rev. B* **71**, 045318 (2005).